Composites: Part A 147 (2021) 106422

Contents lists available at ScienceDirect

Composites Part A

journal homepage: www.elsevier.com/locate/compositesa

Effect of curvature on extensional stiffness matrix of 2-D braided composite tubes

Hemanth Thandaga Nagaraju, Bhavani V. Sankar *, Ghatu Subhash, Nam Ho Kim, Raphael T. Haftka [1]

Department of Mechanical and Aerospace Engineering, University of Florida, Gainesville, FL, USA

ARTICLE INFO

Keywords:
Braided composite tubes
Stiffness matrix
Curvature effect
Micro-mechanics

ABSTRACT

In the micromechanical analysis of braided composite tubes, the effects of curvature are often ignored. This approach is acceptable for thin-walled tubes with a large radius. However, in case of small diameter thick-walled tubes, such an approach may lead to inaccurate results. Therefore, it is of interest to determine when the curvature effects of tubular geometry become important in micromechanics. In this study, the extensional stiffness matrix of 2-D braided composite tubes was calculated using a curved unit-cell. The periodicity was imposed in circumferential and longitudinal directions of the tube. The extensional stiffness coefficients were calculated by simulating an internal pressure test, uniaxial tensile test, and torsion test. The obtained stiffness coefficients were compared to those obtained using a flat unit-cell. The results of curved unit-cell were different from that of flat unit-cell. The differences in stiffness coefficients, calculated using curved and flat unit cells were as high as 13%.

1. Introduction

Braided composite tubes are useful structural components in various fields of engineering. Some of the known applications include braided air ducts, aircraft structural parts, automotive shafts, braided catheters, braided stents, hip prosthesis and braided dental posts [1–3]. The silicon carbide fiber/silicon carbide matrix (SiC/SiC) braided composite tubes are of special interest to the nuclear industry. These composite tubes have desirable properties for a cladding material which requires high resistance to neutron irradiation, high chemical inertness, and enhanced fracture toughness. They are seen as a candidate material to replace the currently used zirconium alloy [4,5]. These tubes have small inner radius ($a = 4 – 7$ mm) and a large wall thicknesses ($t = 1.5–2.5$ mm) and consequently have a high thickness to inner radius ratio wherein the thin-walled assumption is not valid. In addition, the effect of curvature of the tube must be examined for accurate analysis. The evaluation of constitutive relationship of these braided composite tubes is useful not only in understanding their behavior but also in optimizing their performance. The finite element (FE) micromechanical analysis of textile composites is often done by employing a repeatable unit cell (RUC) rather than a whole structure [6,7]. The periodic boundary conditions are then imposed on the FE mesh of the RUC. There are research works that analyze the braided tubes using a flat RUC, which ignore the tubular geometry of the braided composite [8–11]. This is partly due to the non-availability of pre-processing software that can generate FE mesh of curved RUC. Moreover, the FE analysis carried out by employing flat RUC has been found to be reasonably accurate for braided tubes of large diameter. However, this approach might yield questionable results for braided tubes of a small diameter wherein the effects of tubular geometry could be pronounced due to its high ratio of thickness to inner radius (t/a). In this work, we intend to evaluate the influence of t/a on the stiffness coefficients of a textile composite.

There are few research works that allude to the difference in analyzing flat and tubular RUC [1,12,13]. Ayranci et al. evaluated the stiffness of braided composite tubes based on volume averaging of the constituent stiffnesses [1]. In this model, the curved unit cell was divided into three regions namely, matrix-only regions, undulating regions of yarn and non-undulating regions of yarn. The stiffness matrices of individual regions were calculated based on classical lamination theory, which was modified for woven structures. The stiffness matrix of the woven structure was calculated as the sum of stiffness matrices of individual regions. In the above analysis iso-strain conditions within the RUC were implied. There are works in literature that have successfully used iso-strain based models to predict the effective elastic constants of

* Corresponding author.
E-mail address: sankar@ufl.edu (B.V. Sankar).
[1] Deceased on August 16, 2020.

https://doi.org/10.1016/j.compositesa.2021.106422
Received 2 February 2021; Received in revised form 7 April 2021; Accepted 10 April 2021
Available online 15 April 2021

flat braided composites, such as Quek et al. and Kier et al.[14,15]. However, the iso-strain assumption may not hold good for some of the material properties like transverse Young's moduli and shear moduli. An accurate FE analysis would require implementation of periodicity on tubular unit cell as considered in some of the works in literature [12,13]. These works impose periodicity in all three directions, radial, circumferential, and longitudinal directions, of the tube. One of the findings of Chatzigeorgiou et al. [12] is that unit cells in both flat and tubular structures reduce to a cube despite the differences between cylindrical coordinate system and cartesian coordinate system. However, in the case of SiC/SiC cladding material, there are only one or two plies, meaning that the RUC does not have periodic conditions along the thickness direction. In addition, the thickness and inner radius are of the same order of magnitude. For such thick tubes, we propose a methodology to calculate the extensional stiffness coefficients. The extensional stiffness matrix, $[A]$ is calculated for the tubular FE model by imposing displacement periodicity only in circumferential and longitudinal directions of the tube, while no such restriction is specified in the radial direction. This calculation is repeated for tubes of varying inner diameter but same thickness. The calculated stiffness values are then compared with stiffness value predicted by the flat FE model, thus enabling us to assess the influence of t/a on extensional stiffness coefficients.

The paper is organized as follows. In Section 2, the traditional methodology to analyze braided composites by means of flat RUC is briefly described. A novel method to obtain the FE mesh of curved RUC is presented in Section 3 which also includes the equations to impose periodicity on the tubular FE model, the mathematical expressions to calculate force resultants, and macro-stresses and macro-strains pertinent to FE model of the curved RUC. The results are discussed in Section 4, and conclusions are presented in Section 5.

2. Micro-mechanics of flat RUC

The method for evaluating the extensional stiffness matrix $[A]$ of textile composites is discussed in a series of papers by Sankar et al. [7,16,17]. In this paper, the procedures for calculating $[A]$ matrix from a flat unit cell are described briefly for the sake of completeness. The $[A]$ matrix gives the relationship between the force resultants (N_x, N_y, N_{xy}) and mid-plane strains $(\varepsilon_{x0}, \varepsilon_{y0}, \gamma_{xy0})$ for a flat braided textile composite as [18]:

$$\begin{bmatrix} N_x \\ N_y \\ N_{xy} \end{bmatrix} = \begin{bmatrix} A_{11} & A_{12} & A_{16} \\ A_{12} & A_{22} & A_{26} \\ A_{16} & A_{26} & A_{66} \end{bmatrix} \begin{Bmatrix} \varepsilon_{x0} \\ \varepsilon_{y0} \\ \gamma_{xy0} \end{Bmatrix} \tag{1}$$

A rectangular cartesian coordinate system is used to analyze flat FE models. The $[A]$ matrix is evaluated by imposing periodic boundary conditions in two directions (for instance, x and y) only. The boundary faces normal to the third direction (z-axis) do not have any displacement restriction in this analysis. The $[A]$ matrix can also be calculated from the elastic constants that are obtained by imposing periodicity in all three directions. These two methods are discussed in Section 2.1 and Section 2.2, respectively.

2.1. Calculation of $[A]$ matrix using in-plane periodicity

In classical lamination theory, the $[A]$ matrix of a thin laminate is calculated by assuming plane stress assumption in the thickness direction. The meso-structure of the material is assumed to repeat only in the x and y directions. This assumption is valid in analysis of a single layer textile composite where the unit-cell does not repeat in the thickness direction. The periodic boundary conditions imposed on the RUC depicted in Fig. 1 are:

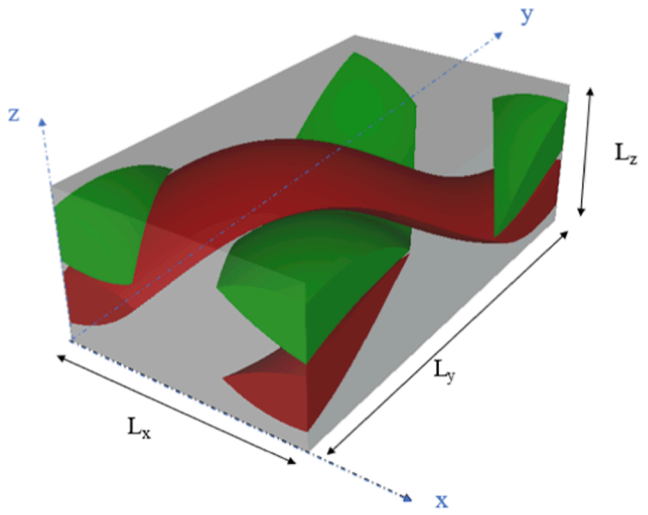

Fig. 1. Flat RUC of the braided composite with the coordinate system. The red and green regions represent the yarns and the remaining grey region is the matrix. (For interpretation of the references to colour in this figure legend, the reader is referred to the web version of this article.)

$$\begin{aligned} u_x(L_x, y, z) - u_x(0, y, z) &= \epsilon_{x0} L_x \\ u_y(L_x, y, z) - u_y(0, y, z) &= \frac{\gamma_{xy0}}{2} L_x \\ u_z(L_x, y, z) - u_z(0, y, z) &= 0 \\ u_x(x, L_y, z) - u_x(x, 0, z) &= \frac{\gamma_{xy0}}{2} L_y \\ u_y(x, L_y, z) - u_y(x, 0, z) &= \epsilon_{y0} L_y \\ u_z(x, L_y, z) - u_z(x, 0, z) &= 0 \end{aligned} \tag{2}$$

In Eq. (2), $L_x$and L_y are the dimensions in the x and y directions of the RUC, respectively, u_i denotes the displacement in respective coordinate direction ($i = x,y,z$), and the strains ε_{x0}, ε_{y0}, γ_{xy0} are the macroscopic mid-plane strains applied to the RUC. The aforementioned periodic boundary conditions are imposed on the FE model using multipoint constraints in ABAQUS software [19,20]. The $[A]$ matrix is evaluated by carrying out three FE simulations. In each of these simulations, the boundary conditions are applied such that only one of the mid-plane strains is non-zero. The resulting stresses and strains in individual elements of FE model are called micro-stresses and micro-strains, respectively. The micro-stresses are averaged to obtain force resultants (N_x, N_y, N_{xy}) as follows [7,16]:

$$\begin{aligned} N_x &= \frac{1}{L_x L_y} \int \sigma_x^e \, dv = \frac{\sum_{e=1}^{n} v^e \sigma_x^e}{L_x L_y} \\ N_y &= \frac{1}{L_x L_y} \int \sigma_y^e \, dv = \frac{\sum_{e=1}^{n} v^e \sigma_y^e}{L_x L_y} \\ N_{xy} &= \frac{1}{L_x L_y} \int \tau_{xy}^e \, dv = \frac{\sum_{e=1}^{n} v^e \tau_{xy}^e}{L_x L_y} \end{aligned} \tag{3}$$

The averaging is done numerically. In Eqs. (3), n is the total number of elements in the FE model, $\sigma_x^e, \sigma_y^e, \tau_{xy}^e$ are the micro-stresses in element e and v^e is the volume of element e. The mid-plane strains can be calculated by averaging the micro-strains as:

$$\varepsilon_{x0} = \frac{1}{L_x L_y}\int \varepsilon_x^e \, dv = \frac{\sum_{e=1}^{n} v^e \varepsilon_x^e}{L_x L_y}$$

$$\varepsilon_{y0} = \frac{1}{L_x L_y}\int \varepsilon_y^e \, dv = \frac{\sum_{e=1}^{n} v^e \varepsilon_y^e}{L_x L_y} \quad (4)$$

$$\gamma_{xy0} = \frac{1}{L_x L_y}\int \gamma_{xy}^e \, dv = \frac{\sum_{e=1}^{n} v^e \gamma_{xy}^e}{L_x L_y}$$

where ε_x^e, ε_y^e, γ_{xy}^e represent the strains (micro-strains) of element e. The mid-plane strains calculated using Eqs. (4) should be equal to the applied macrostrains. The calculated force

resultants and mid-plane strains are then substituted in Eq. (1) and solved for the unknown extensional stiffness coefficients. The A_{ij} coefficients, in the first column of $[A]$ matrix are calculated through an FE simulation in which mid-plane strain ε_{x0}, is the only non-zero component of mid-plane strains. Similarly, the A_{ij} coefficients in the second and third column of $[A]$ matrix (Eq. (1)) are calculated through FE simulations in which ε_{y0} and γ_{xy0} are the only non-zero components of mid-plane strains, respectively. The detailed procedure can be found in the works of Marrey et al. [7,16,17].

2.2. Calculation of [A] matrix from three-dimensional elastic constants

In this method, it is assumed that the unit cell repeats in all three directions. Hence, the periodic boundary conditions are imposed in x, y and z directions. The detailed procedure can be found elsewhere [7,21]. The three-dimensional periodic boundary conditions are [7]:

$$u_x(L_x,y,z) - u_x(0,y,z) = \varepsilon_x L_x$$

$$u_y(L_x,y,z) - u_y(0,y,z) = \frac{\gamma_{xy}}{2} L_x$$

$$u_z(L_x,y,z) - u_z(0,y,z) = \frac{\gamma_{xz}}{2} L_x$$

$$u_x(x,L_y,z) - u_x(x,0,z) = \frac{\gamma_{xy}}{2} L_y$$

$$u_y(x,L_y,z) - u_y(x,0,z) = \varepsilon_y L_y \quad (5)$$

$$u_z(x,L_y,z) - u_z(x,0,z) = \frac{\gamma_{yz}}{2} L_y$$

$$u_x(x,y,L_z) - u_x(x,y,0) = \frac{\gamma_{xz}}{2} L_z$$

$$u_y(x,y,L_z) - u_y(x,y,0) = \frac{\gamma_{yz}}{2} L_z$$

$$u_z(x,y,L_z) - u_z(x,y,0) = \varepsilon_z L_z$$

The strains in Eq. (5) are macroscopic components. The stiffness matrix $[C]_{6X6}$ is calculated through six FE simulations under periodic boundary conditions. In each of these six FE analyses, only one component of macrostrain is chosen to be non-zero. In post-processing, resulting micro-stresses and micro-strains are volume averaged to obtain macrostresses and macrostrains respectively, using the following equations:

$$\sigma_{ii} = \frac{1}{V}\int \sigma_{ii} \, dv = \frac{\sum_{K=1}^{n} v^e \sigma_{ii}^e}{V}$$

$$\varepsilon_{ii} = \frac{1}{V}\int \varepsilon_{ii} \, dv = \frac{\sum_{K=1}^{n} v^e \in_{ii}^e}{V} \quad (6)$$

where $V$is the volume of RUC. The calculated macrostresses and applied macrostrains are substituted into the constitutive relation:

$$\{\sigma\}_{6\times1} = [C]_{6\times6}\{\varepsilon\}_{6\times1} \quad (7)$$

where $\{\sigma\}$ is the vector of macrostresses, $\{\varepsilon\}$ is the vector of macrostrains and $[C]$ is the stiffness matrix. The column of stiffness matrix corresponding to the only non-zero macrostrain is then calculated. Thus, all the columns of stiffness matrix are calculated by six independent loading conditions.

The lamina stiffness matrix $[Q]$, can then be calculated from the compliance matrix, which is the inverse of the above stiffness matrix, $\left([S] = [C]^{-1}\right)$ using plane stress assumption [18,22]:

$$Q_{11} = \frac{S_{22}}{S_{11}S_{22} - S_{12}^2} = \frac{E_x}{1 - \nu_{xy}\nu_{yx}}$$

$$Q_{12} = \frac{-S_{12}}{S_{11}S_{22} - S_{12}^2} = \frac{E_x\nu_{xy}}{1 - \nu_{xy}\nu_{yx}} \quad (8)$$

$$Q_{22} = \frac{S_{11}}{S_{11}S_{22} - S_{12}^2} = \frac{E_y}{1 - \nu_{xy}\nu_{yx}}$$

$$Q_{66} = \frac{1}{S_{66}} = \frac{1}{G_{xy}}$$

The extensional stiffness matrix $[A]$ is calculated as the product of the lamina stiffness matrix $[Q]$ and thickness h of the textile composite [22]:

$$[A] = h[Q] \quad (9)$$

3. Micro-mechanics of curved RUC

The mapping procedure employed to obtain FE mesh of curved RUC is explained in Section 3.1. The mapping scheme is verified in Section 3.2 by considering hoop stress in a homogeneous isotropic tube under internal pressure. In Section 3.3, the periodic boundary conditions pertinent to curved RUC and the calculation of $[A]$ matrix are discussed. The implementation of periodic boundary conditions is verified by considering the radial displacement of a homogeneous isotropic tube under internal pressure in the plane stress state.

3.1. Mapping of flat RUC into curved RUC

The flat FE model of braided textile composites can be obtained from software packages such as WiseTex and TeXGen. In this study, the FE mesh of flat RUC was generated using the open source geometric modeling software "TeXGeN" [23,24]. TeXGeN generates an FE mesh that is homologous which is necessary for the successful implementation of periodic boundary conditions [25,26]. The node sets that identify the nodes at corresponding points on opposite faces, edges, and corner vertices of the FE mesh, are defined in a TeXGen generated input file. This is helpful in implementing periodic boundary conditions. An eight-node brick element (linear hexahedron) with a reduced integration scheme (C3D8R) in ABAQUS software was employed in this analysis. The yarn is modeled as a homogeneous orthotropic material and the matrix is treated as a homogeneous isotropic material. The FE mesh of the curved RUC is obtained by mapping the nodal coordinates of the flat RUC to that of the curved RUC using the following equations:

$$\begin{aligned} r &= R_m + z - L_z/2 \\ \phi &= \frac{x}{R_m} \\ x' &= r\sin(\phi) \\ y' &= y \\ z' &= r\cos(\phi) \end{aligned} \tag{10}$$

where (x, y, z) denote the coordinates of flat RUC and (x', y', z') are nodal coordinates of FE mesh of the curved RUC. The mean radius of the tube is represented by R_m. This mapping is pictorially represented in Fig. 2. The mapping is applied to each node in the flat RUC to find the location of the corresponding node in the curved RUC. The finite element definitions and connectivity of FE model of tubular RUC remain unchanged from that of the flat RUC. In this mapping procedure, the volume of elements in the top half of the RUC is increased while that of those in the bottom half is decreased. However, the volume of the whole RUC and yarn volume fraction remain the same. This is achieved by specifying the path of the yarn so that, yarn is equally distributed in top half and bottom half of flat RUC.

While exporting the FE model of flat RUC, TeXGen generates two files in addition to ABAQUS input file. One of them contains the element data (file with .eld extension) and the other file (with .ori extension) contains information about the orientation of yarn elements. The orientation has two unit vectors defined at the center of each finite element. In yarn element, one vector is aligned along the path of the yarn and the other is oriented perpendicular to the first. These unit vectors are used to define the orientation of yarn finite elements. The unit vectors, that are parallel to the path of yarn are schematically shown in Fig. 3. During the mapping, from flat RUC to curved RUC, the FE elements are bent about the y-axis, hence the following vector transformation is used to obtain the orientation of the yarn finite elements in the curved RUC.

$$T = \begin{bmatrix} \cos\varphi_c & 0 & \sin\varphi_c \\ 0 & 1 & 0 \\ -\sin\varphi_c & 0 & \cos\varphi_c \end{bmatrix} \tag{11}$$

$$\begin{pmatrix} a' \\ b' \\ c' \end{pmatrix} = [T] \begin{pmatrix} a \\ b \\ c \end{pmatrix} \tag{12}$$

where φ_c is the transformation angle corresponding to the geometric centroid of the yarn element. The direction cosines of the vector in the curved RUC are (a', b', c'), while (a, b, c) are the direction cosines of the vector in the flat RUC.

3.2. Verification of the mapping procedure

It is imperative that the designed mapping scheme produces an FE mesh of tubular RUC with desired curvature and thickness. This was verified by comparing hoop stress calculated by the FE analysis of homogeneous isotropic tube under internal pressure, with analytical solution from elasticity. The mapping scheme defined by Eq. (10) was used to obtain the FE model of curved RUC. A cylindrical coordinate system (r, θ, y), whose origin is at the geometric center of the tube is used to analyze curved RUC. To model a homogeneous isotropic tube, elastic constants of the constituent yarn and matrix elements of curved RUC were defined by the same value. The boundary conditions can be explained with the help of Fig. 4. The circumferential planes of the tubular RUC are not allowed to have any tangential displacements while planes normal to the longitudinal direction are not allowed to have any longitudinal displacement, meaning that isotropic tube is subjected to internal pressure under plane strain state. These boundary conditions are mathematically expressed by the following equations in cylindrical coordinate system (r, θ, y):

$$\begin{aligned} u_r(r, -\alpha, y) &= 0 \\ u_r(r, \alpha, y) &= 0 \\ u_\theta\left(r, \theta, \frac{-L_y}{2}\right) &= 0 \\ u_\theta\left(r, \theta, \frac{L_y}{2}\right) &= 0 \end{aligned} \tag{13}$$

In Eq. (13), u_r and u_θ denote tangential and longitudinal displacements, respectively, while α is half of the angle subtended by the tube at its center (see Fig. 2) and L_y is the length of the curved RUC in the y-direction (see Fig. 4). The hoop stress generated in a homogeneous isotropic tube due to internal pressure p is given by the following analytical solution obtained from elasticity theory [27]:

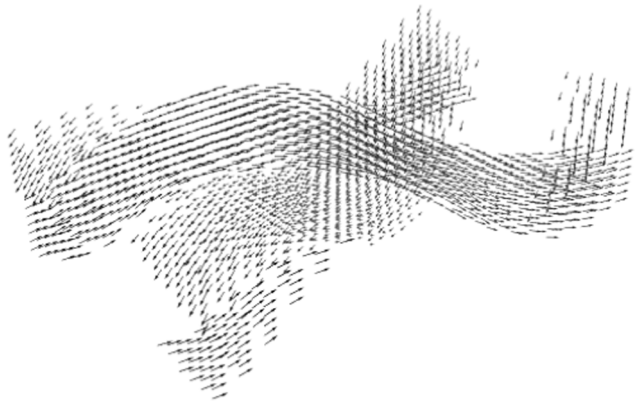

Fig. 3. The unit vectors (represented by line segments with an arrow) of yarn finite elements, parallel to the path of the yarn. These vectors are used to define the material coordinate system of flat RUC.

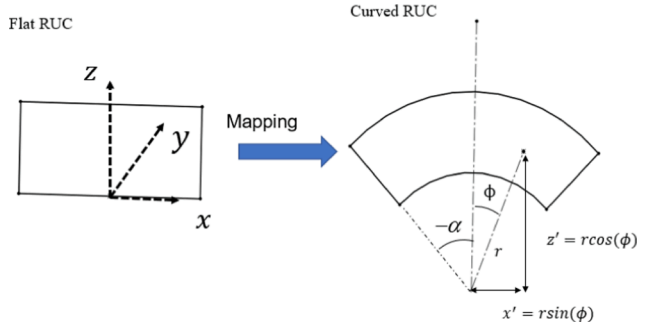

Fig. 2. Mapping the nodal coordinates of FE mesh of flat RUC to that of curved RUC. (For interpretation of the references to colour in this figure legend, the reader is referred to the web version of this article.)

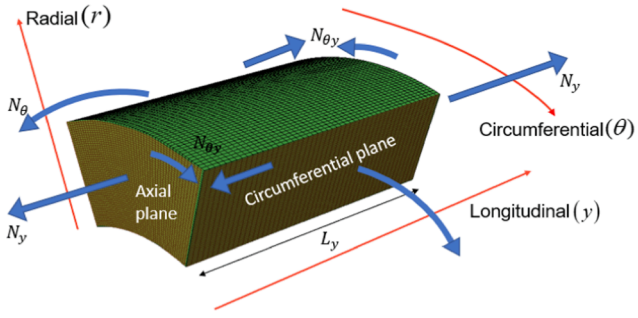

Fig. 4. The force resultants and boundary planes pertinent to curved RUC. (For interpretation of the references to colour in this figure legend, the reader is referred to the web version of this article.)

$$\sigma_{hoop} = \frac{a^2 p}{b^2 - a^2}\left(1 + \frac{b^2}{r^2}\right) \tag{14}$$

where a and b are inner and outer radii of the tube, r is the distance between the point of interest and the center of the tube. The results of this exercise are presented in the following.

The purpose here is to ensure accurate implementation of mapping equations given by Eq. (10). The tube was subjected to an internal pressure $p = 100$ MPa. The hoop stresses from FE analysis were compared with those from the analytical solution (Eq. (14)), as shown in Fig. 5. It is seen that there is an excellent agreement between the two. This result demonstrates that the mapping scheme given by Eq. (10) are correctly implemented.

3.3. Periodic boundary conditions and calculation of $[A]$ matrix

The boundary conditions represented by Eq. (13) in Section 3.2 are suitable only if the boundary (longitudinal and circumferential) planes remain as planes after deformation. These boundary conditions do not necessarily impose periodicity which is required in the analysis of a heterogeneous braided composite tube. There are few works in the literature in which imposing periodicity onto tubular FE models in all three directions is discussed [12,13]. However, in SiC/SiC composite tubes with just one or two plies, the periodicity does not apply in the radial direction. In the present work, periodic boundary conditions are imposed on a tubular RUC by using a cylindrical coordinate system (r, θ, y) whose origin is located at the geometric center of the tube. The periodicity is imposed in circumferential and longitudinal directions only to calculate the extensional stiffness coefficients. The outer and inner cylindrical surfaces do not have any displacement restrictions, as defined in the following equations:

$$u_r(r, -\alpha, y) - u_r(r, \alpha, y) = 0 \tag{15}$$

$$u_\theta(r, -\alpha, y) - u_\theta(r, \alpha, y) = 0 \tag{16}$$

$$u_y(r, -\alpha, y) - u_y(r, \alpha, y) = 0 \tag{17}$$

$$u_r\left(r, \theta, -\frac{L_y}{2}\right) - u_r\left(r, \theta, \frac{L_y}{2}\right) = 0 \tag{18}$$

$$u_\theta\left(r, \theta, -\frac{L_y}{2}\right) - u_\theta\left(r, \theta, \frac{L_y}{2}\right) = \frac{\gamma_{\theta y0}}{b} r L_y \tag{19}$$

$$u_y\left(r, \theta, -\frac{L_y}{2}\right) - u_y\left(r, \theta, \frac{L_y}{2}\right) = \epsilon_{y0} L_y \tag{20}$$

To impose periodic boundary conditions, dummy nodes outside the FE model are used as reference points. The appropriate displacement component is then specified on these reference points. For instance, to impose Eq. (15), u_r displacement of the reference point corresponding to Eq. (15) is set to zero. The periodic boundary equations are imposed on curved RUC through linear constraint equations in the ABAQUS software by employing a cylindrical coordinate system [19].

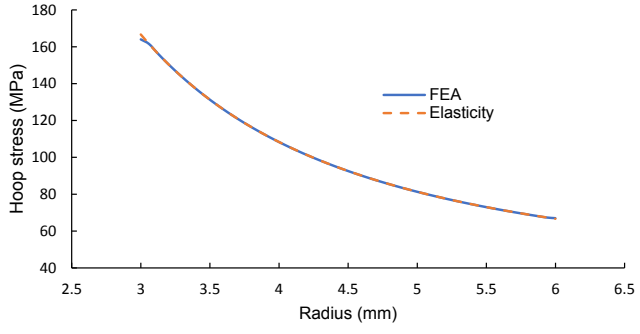

Fig. 5. Comparison of hoop stress in a homogeneous isotropic tube between FE result and analytical solution. (For interpretation of the references to colour in this figure legend, the reader is referred to the web version of this article.)

The objective is to calculate the extensional stiffness matrix $[A]$ while using Eqs. (15)–(20) to impose periodicity on the curved RUC. The extensional stiffness matrix of the composite tube gives the relationship between the force resultants $(N_\theta,\ N_y,\ N_{\theta y})$ and mid-plane strains $(\varepsilon_{\theta 0},\ \varepsilon_{y0},\ \gamma_{\theta y0})$ as:

$$\begin{Bmatrix} N_\theta \\ N_y \\ N_{\theta y} \end{Bmatrix} = \begin{bmatrix} A_{11} & A_{12} & A_{16} \\ A_{12} & A_{22} & A_{26} \\ A_{16} & A_{26} & A_{66} \end{bmatrix} \begin{Bmatrix} \varepsilon_{\theta 0} \\ \varepsilon_{y0} \\ \gamma_{\theta y0} \end{Bmatrix} \tag{21}$$

The coefficients A_{16} and A_{26} are expected to vanish as the normal and shear deformations are decoupled. The coefficient A_{11} is the stiffness along the circumferential direction, A_{22} is the stiffness in the longitudinal direction of the tube, A_{12} is the Poisson effect between the circumferential and longitudinal direction of the tube, and A_{66} coefficient is a measure of the torsional stiffness. An alternative form of Eq. (21) is given by:

$$\begin{Bmatrix} \varepsilon_{\theta 0} \\ \varepsilon_{y0} \\ \gamma_{\theta y0} \end{Bmatrix} = \begin{bmatrix} a_{11} & a_{12} & 0 \\ a_{12} & a_{22} & 0 \\ 0 & 0 & a_{66} \end{bmatrix} \begin{Bmatrix} N_\theta \\ N_y \\ N_{\theta y} \end{Bmatrix} \tag{22}$$

where $[a] = [A]^{-1}$. The force resultants are pictorially represented in Fig. 4. The $[a]$ matrix is calculated using the FE model of curved RUC by simulating three tests - internal pressure test (a_{11}), uniaxial tensile test (a_{12}, a_{22}) and torsion test (a_{66}).

To simulate the internal pressure test (plane stress in the longitudinal direction), Eqs. (15)–(20) are imposed on curved FE mesh with $\gamma_{\theta y0} = 0$ which is imposed by specifying the u_θ displacement on the reference point corresponding to Eq. (19) as zero. However, the u_y displacement on the reference point corresponding to Eq. (20) is set free, which allows the curved RUC to contract longitudinally if needed such that the corresponding longitudinal force resultant, $N_y = 0$. The deformation of curved RUC is driven by an internal pressure acting on the inner cylindrical surface of composite tube. Thus, N_θ is the only non-zero force resultant and $a_{11} = \frac{\varepsilon_{\theta 0}}{N_\theta}$. To simulate uniaxial tension in the longitudinal direction, Eqs. (15)–(20) are imposed on curved RUC with $\varepsilon_{y0} \neq 0$, which is achieved by specifying an arbitrary u_y on the reference point corresponding to (20). The mid-plane shear strain is set to zero ($\gamma_{\theta y0} = 0$), as there is no coupling between the normal strain component and shear stresses, the force resultant $N_{\theta y}$ is zero. In this simulation N_y is the only non-zero force resultant. The coefficients $a_{12}$and a_{22} are calculated as $\frac{\varepsilon_{\theta 0}}{N_y}$ and $\frac{\varepsilon_{y0}}{N_y}$ respectively. Finally, the torsion test is simulated by imposing Eqs. (15)–(20) with $\gamma_{\theta y} \neq 0$, $\epsilon_y = 0$, and no internal pressure. The shear force resultant $N_{\theta y}$ is the only non-zero force resultant in torsion. The coefficient $a_{66} = \frac{\gamma_{\theta y0}}{N_{\theta y}}$. Once $[a]$ is evaluated for the tubular geometry, its inverse gives the extensional stiffness matrix, $[A]$ of braided tubes.

The implementation of periodic boundary conditions given by Eqs. (15)–(20) must be verified. For this purpose, the radial displacement of a homogeneous isotropic tube under internal pressure given by FE analysis is compared with the analytical solution from elasticity [27]:

$$u_r = \frac{a^2 p r}{E\left(b^2 - a^2\right)}\left((1 - \nu) + (1 + \nu)\frac{b^2}{r^2}\right) \tag{23}$$

where,E is Young's modulus and ν is Poisson's ratio whose values were chosen to be 200 GPa and 0.3, respectively. The comparison between FE analysis and the analytical solution for radial displacements due to internal pressure under plane stress is shown in Fig. 6. It can be observed that the FE results agree well with the analytical results. The good agreement between the two solutions gives us confidence that the

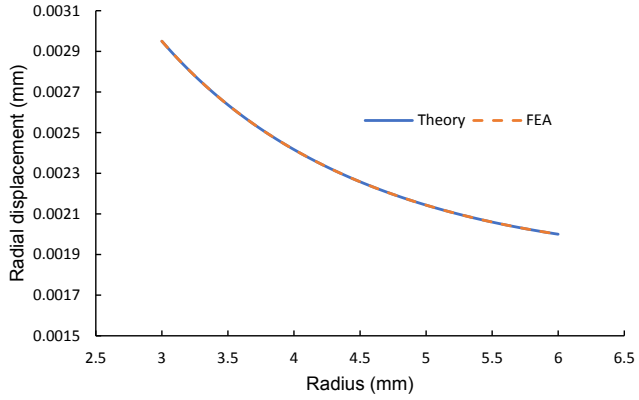

Fig. 6. Comparison of radial displacement from FE and analytical solution for a homogeneous isotropic tube. (For interpretation of the references to colour in this figure legend, the reader is referred to the web version of this article.)

periodic boundary conditions were appropriately

implemented in the longitudinal and circumferential directions of curved RUC. Thus, the Eqs. (15)–(20) can be employed to analyze a heterogeneous braided composite tube.

In analyzing the flat RUC, micro-stresses and micro-strains are volume averaged to get force resultants and mid-plane strains as discussed in Section 2 and as per Eqs. (3), (4) and (6) [6,7]. However, the volume averaging of micro-stresses and micro-strains does not yield force resultant and mid-plane strains in curved RUC. The formulae to calculate force resultants $(N_\theta,\ N_y,\ N_{\theta y})$ and mid-plane strains $(\varepsilon_{\theta 0},\ \varepsilon_{y0},\ \gamma_{\theta y0})$ from FE analysis of curved RUC is derived in the rest of the section. As an example, let us consider the micro-stress σ_θ^μ . The corresponding force resultant N_θ is derived as described in the following. First, the force resultant $\widetilde{N}_\theta$at a given $(\theta, y)$is derived by integrating σ_θ^μ through the thickness:

$$\widetilde{N}_\theta(\theta,y) = \int_a^b \sigma_\theta^\mu(r,\theta,y)dr \tag{24}$$

The above force resultant is then averaged over the entire RUC to obtain the macro-force resultant as:

$$\begin{aligned} N_\theta &= \frac{1}{2\alpha L_y}\int_0^{L_y}\int_{-\alpha}^{+\alpha}\widetilde{N}_\theta(\theta,y)d\theta dy \\ &= \frac{1}{2\alpha L_y}\int_0^{L_y}\int_{-\alpha}^{+\alpha}\int_a^b \sigma_\theta^\mu(r,\theta,y)drd\theta dy \end{aligned} \tag{25}$$

The above equation can be modified to facilitate the evaluation of the integral in the FE analysis by multiplying and dividing by the term(R_m/r) :

$$\begin{aligned} N_\theta &= \frac{1}{2\alpha L_y R_m}\int_0^{L_y}\int_{-\alpha}^{+\alpha}\int_a^b \sigma_\theta^\mu(r,\theta,y)\frac{R_m}{r}rdrd\theta dy \\ &= \frac{1}{A_m}\int_0^{L_y}\int_{-\alpha}^{+\alpha}\int_a^b \sigma_\theta^\mu(r,\theta,y)\frac{R_m}{r}dv \end{aligned} \tag{26}$$

where $A_m = 2\alpha L_y R_m$is the area of the mid-surface of the curved RUC. The above volume integral is evaluated in the FE analysis as:

$$N_\theta = \frac{R_m}{A_m}\sum_{e=1}^{n}\frac{\sigma_\theta^{(e)}v^{(e)}}{r^{(e)}} \tag{27}$$

where $\sigma_\theta^{(e)}$ is the hoop stress in the element e, with volume $v^{(e)}$. Similarly, one can derive an expression for mid-plane strain$\varepsilon_{\theta 0}$:

$$\begin{aligned} \varepsilon_{\theta 0} &= \frac{1}{2\alpha L_y R_m(b-a)}\int_0^{L_y}\int_{-\alpha}^{+\alpha}\int_a^b \varepsilon_\theta(r,\theta,z)\frac{R_m}{r}dv \\ &= \frac{R_m}{V}\sum_{e=1}^{n}\frac{\varepsilon_\theta^{(e)}v^{(e)}}{r^{(e)}} \end{aligned} \tag{28}$$

In Eqs. (27) and (28), $r^{(e)}$ is the radius of the element e, V is the volume of RUC and n is the total number of elements in FE mesh.

The $[A]$ matrix was evaluated for various t/a values by changing inner radius a of the tube, but maintaining a constant tube thickness. The obtained extensional stiffness values of the composite tube were then normalized with respect to the stiffness value obtained from 3D elastic constants described in Section 2.2. The yarn volume fraction and thickness of tubes were maintained at 0.298 and 3 mm, respectively. The stiffness values of the curved RUCs were compared to that of flat RUCs. The plots of the normalized stiffness values versus the ratio of thickness to inner radius are presented and discussed in the next section.

4. Results and discussion

In this study, extensional stiffness matrices of two-dimensionally braided biaxial composite tubes were evaluated. A braid angle of 30 degree was chosen. Two composite material systems, SiC/SiC and carbon/epoxy, were considered. The elastic constants of SiC/SiC and carbon/epoxy material are given in Table 1 and Table 2, respectively. Note that the carbon/epoxy composite is more anisotropic $\left(\frac{E_1}{E_2} \cong 6\right)$ compared to the SiC/SiC $\left(\frac{E_1}{E_2} \cong 2\right)$ composite. Also note that matrix properties are dominant in SiC/SiC material system while the yarn properties are dominant in carbon/epoxy material system. This choice of property will help us assess the effect of tubular geometry with

heterogeneity on two kinds of braided composites: matrix dominant and yarn dominant material systems.

As mentioned in Section 2.1, the extensional stiffness matrix $[A]$ of braided composite tubes calculated using flat RUC does not reflect the effect of tube radius. To account for tubular geometry, the extensional stiffness matrix $[A]$ was calculated by imposing periodicity on the curved RUC as discussed in Section 3. The extensional stiffness coefficients are presented in Table 3 and Table 4, respectively, for SiC/SiC and carbon/epoxy material systems for various values of t/a. The stiffness coefficients were normalized by those elastic constants obtained from stiffness coefficients calculated by imposing periodicity in all three directions of a flat RUC as discussed in Section 2.2 and plotted as a function of t/a in Figures (7–10). In these figures, the primed coefficients $A_{ij}^{'}$ denote the value evaluated by imposing periodicity in two directions only, while the unprimed coefficients A_{ij} denote the value obtained by imposing the periodicity in all three direction of a flat RUC.

The $[A]$ matrix calculated by imposing three-dimensional periodicity on the flat FE model for SiC/SiC is

$$A = \begin{bmatrix} 935,559 & 183,063 & 0 \\ 183,063 & 996,451 & 0 \\ 0 & 0 & 410,538 \end{bmatrix}\frac{\text{N}}{\text{mm}} \tag{29}$$

and for carbon/epoxy is

Table 1
Elastic constants of SiC/SiC composite [28].

Material	Young's moduli (GPa)	Shear moduli (GPa)	Poisson's ratios
SiC/SiC yarn	$E_1 = 259, E_2 = 106 E_3 = 106$	$G_{12} = 41.4, G_{13} = 41.4 G_{23} = 42.5$	$\nu_{12} = 0.21, \nu_{13} = 0.21, \nu_{23} = 0.18$
SiC matrix	$E = 420$	$G = 179.48$	$\nu = 0.17$

Table 2
Elastic constants of carbon/epoxy material system [29].

Material	Young's moduli [GPa]	Shear moduli [GPa]	Poisson's ratios
Carbon/epoxy yarn	$E_1 = 165.7\, E_2 = 27.13,\ E_3 = 27.13$	$G_{12} = 8.88,\ G_{13} = 8.88, G_{23} = 11.59$	$\nu_{12} = 0.204,\ \nu_{13} = 0.204, \nu_{23} = 0.17$
epoxy matrix	$E = 7.52$	$G = 2.76$	$\nu = 0.36$

Table 3
The extensional stiffness coefficients of SiC/SiC braided tube of wall thickness 3 mm.

Inner Radius a (mm)	A_{11}(N/mm)	A_{12}(N/mm)	A_{22}(N/mm)	A_{66}(N/mm)
3	880,148	172,073	984,962	407,004
6	896,773	174,299	985,424	405,531
9	905,029	175,583	985,675	405,103
15	913,148	176,946	985,935	404,832
80	925,483	179,194	986,370	404,652
Flat RUC	928,803	179,830	986,489	404,643

Table 4
The extensional stiffness coefficients of Carbon/epoxy braided tube of wall thickness 3 mm.

Inner Radius a(mm)	A_{11}(N/mm)	A_{12}(N/mm)	A_{22}(N/mm)	A_{66}(N/mm)
3	34,329	16,414	59,034	21,764
6	35,802	16,409	56,954	21,538
9	36,458	16,447	56,267	21,443
15	37,094	16,552	55,846	21,376
80	38,073	16,860	55,662	21,328
Flat RUC	38,341	16,973	55,698	21,326

$$A = \begin{bmatrix} 39,463 & 19,330 & 0 \\ 19,330 & 64,790 & 0 \\ 0 & 0 & 23,995 \end{bmatrix} \frac{\mathrm{N}}{\mathrm{mm}} \tag{30}$$

From Figs. 7–10, we observe that stiffness values calculated by imposing the periodicity in in-plane directions of flat RUC are less than the stiffness values calculated by imposing periodicity in all three directions. When periodicity is imposed in all three directions, no boundary faces are left free of displacement restriction unlike in-plane periodicity where there is no displacement restriction in thickness direction. The periodicity restriction along thickness

direction imposes additional constraint making the material apparently stiffer. This results in higher stresses in individual elements of RUC for unit strains leading to higher values of extensional stiffness coefficients. The trend of normalized stiffness along the circumferential direction A_{11} is shown in Fig. 7. The A_{11} value of curved unit cell was less than that predicted by flat unit cell for both SiC/SiC as well as carbon/epoxy. In analysis of flat RUC, to calculate A_{11} an in-plane displacement is specified. However, in analysis of curved RUC, traction is applied normal to the surface at inner radius along the radial direction. It was observed that this difference in approach results in A_{11} calculated from curved RUC being less than that of flat RUC. The difference was found to be larger for the more anisotropic yarn dominant carbon/epoxy (with 13%) than that of matrix dominant SiC/SiC (with 5%). It is interesting to note that A_{11} from curved RUC approached that of flat RUC asymptotically for matrix dominant SiC/SiC but in case of yarn dominant carbon/epoxy, A_{11} value from curved RUC exceeds the value predicted by flat RUC at one data point albeit by a small amount. A similar trend was observed for stiffness coefficient A_{12}, which measures the Poisson effect between the circumferential and longitudinal directions of tube, is shown in Fig. 8. However, the trend of A_{12} was found to be more nonlinear than that of A_{11}. The trend of coefficient A_{22}, which measures the stiffness in longitudinal direction of tube is shown in Fig. 9. In case of matrix dominant SiC/SiC, the tubular geometry has minimal effect. However, for yarn dominant carbon/epoxy, it was found that flat unit cell underestimates the stiffness when compared to the value predicted by the curved unit cell. The maximum difference in A_{22} for carbon/epoxy was about 5%. Finally, the trend of torsional stiffness A_{66} is shown in Fig. 10. It was observed that tubular geometry has minimal effect on A_{66} in case of SiC/SiC material. However, a flat unit cell would underestimate A_{66} of carbon/epoxy by 4% in extreme scenario with $\frac{t}{a} = 1$.

In this study, the yarn volume fraction remained the same for both SiC/SiC and carbon/epoxy material systems. Even if the yarn volume fraction are changed, the A_{11} and A_{12} coefficients calculated from flat RUC will be higher when compared to that of curved RUC. Furthermore, we expect this effect to hold good even for an architecture of different braiding angle. However, the effect of tubular geometry on A_{22} and A_{66} is inconclusive as it might depend on the material system.

In all the plots observed in Figs. 7-10, the stiffness coefficients show a monotonic trend. The value obtained from curved RUC is either less than or greater than that of flat RUC and the difference between the results of flat RUC and curved RUC keeps increasing with higher t/a values. It is

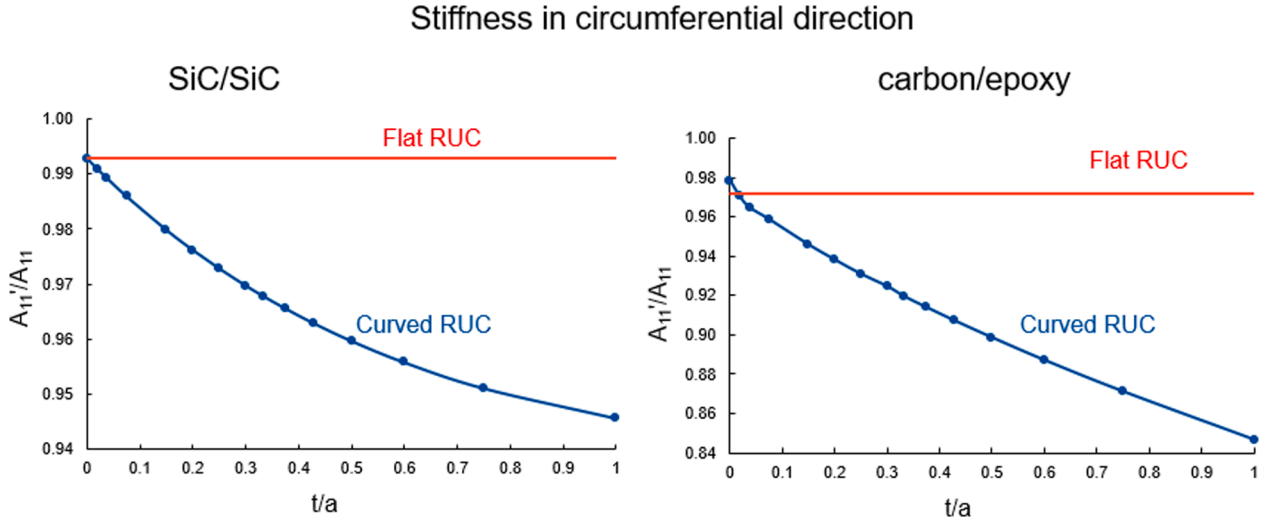

Fig. 7. Trend of normalized A_{11} of SiC/SiC and carbon/epoxy. (For interpretation of the references to colour in this figure legend, the reader is referred to the web version of this article.)

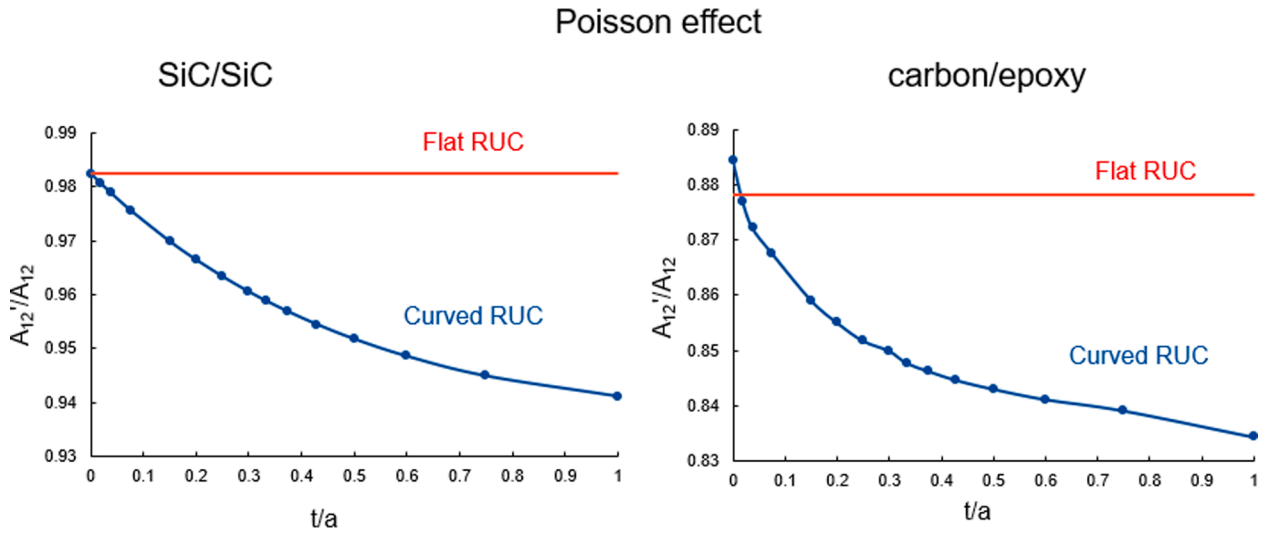

Fig. 8. Trend of normalized A_{12} of SiC/SiC and carbon/epoxy. (For interpretation of the references to colour in this figure legend, the reader is referred to the web version of this article.)

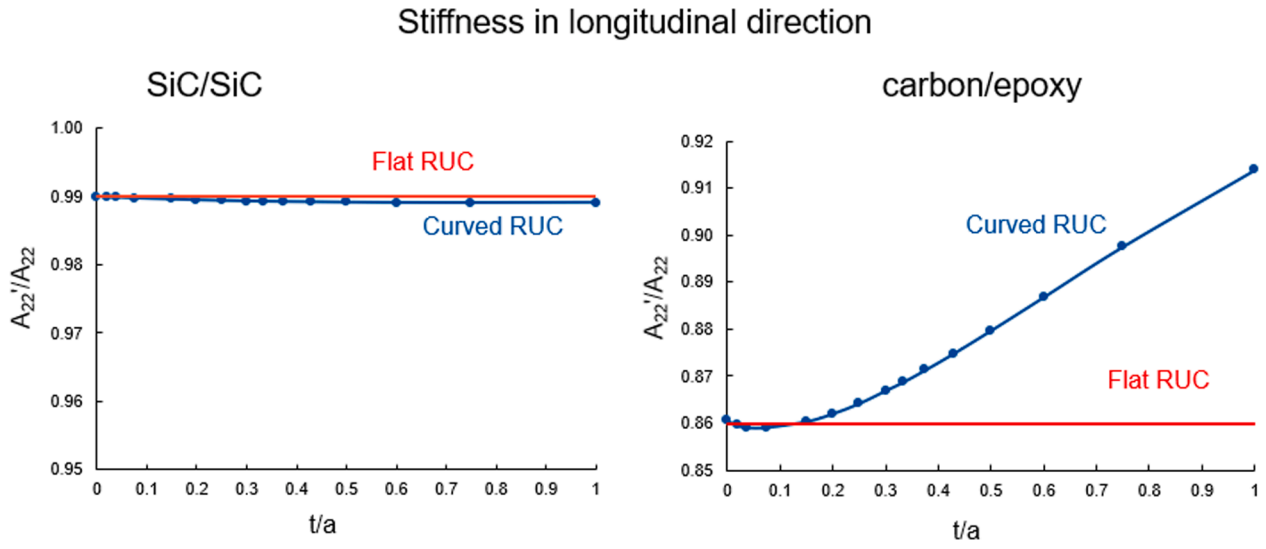

Fig. 9. Trend of normalized A_{22} of SiC/SiC and carbon/epoxy. (For interpretation of the references to colour in this figure legend, the reader is referred to the web version of this article.)

conjectured that the same trend will continue beyond $\frac{t}{a} = 1$.

In summary, it can be said that employing flat RUC to analyze braided composite tubes will lead to overestimation of the coefficients A_{11} and A_{12}, while the trend of coefficients A_{22} and A_{66} depend on the type of material. It was further observed that difference in extensional stiffness coefficients due to tubular geometry is more pronounced in case of more anisotropic carbon/epoxy material. However, all the stiffness coefficients of braided tube approach the value calculated by using flat RUC as $t/a \rightarrow 0$, as observed in Figs. 7-10. Whether the difference in results of curved RUC and flat RUC are significant enough depends on the level of accuracy desired in a particular application. This paper has detailed the procedure or methodology to examine the effect of curvature on stiffness coefficients of braided tubes. An analyst dealing with a critical application like cladding material of a nuclear reactor might be interested in the effect of tubular geometry on extensional stiffness coefficients of braided composite tubes. In that case, the effect of tubular geometry on the $[A]$ matrix can be assessed through micro-mechanics of curved unit cell as discussed in this paper.

5. Conclusions

In this research, finite element mesh of curved unit-cell of a braided composite tube was obtained by using mathematical expressions to map coordinates of FE mesh of the flat unit cell to that of curved unit cell of braided composite tube. The mapping procedure was verified by analyzing the response of homogeneous isotropic tube to internal pressure. The displacement periodic boundary conditions on curved FE mesh and its accuracy was verified by comparing FE solution with analytical solution for thick-walled homogeneous isotropic tubes under internal pressure in plane stress state. The extensional stiffness matrix was evaluated for a 2D biaxial braided composite tube with braid angle of 30 degrees for varying inner radius but same thickness. The extensional stiffness matrix [A] of tubes was then compared with [A] matrix obtained from flat geometry of textile composite. It was found that for thick-walled small diameter tubes, the [A] matrix of tubular geometry is different from that of flat geometry by 5% to 13% (for $(t/a) > 0.5$). However, the stiffness coefficients of tubular geometry were close to that of flat geometry for sufficiently thin tubes $(t/a < 0.1)$.

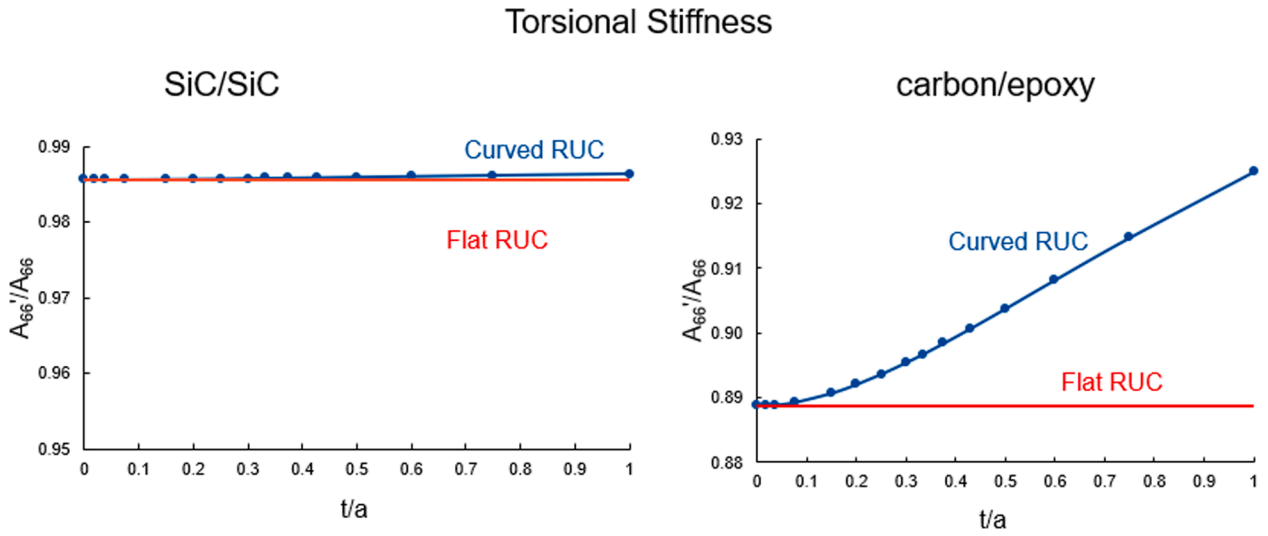

Fig. 10. Trend of normalized A_{66} of SiC/SiC and carbon/epoxy. (For interpretation of the references to colour in this figure legend, the reader is referred to the web version of this article.)

CRediT authorship contribution statement

Hemanth Thandaga Nagaraju: Methodology, Formal analysis, Data curation, Investigation, Writing - original draft. **Bhavani V. Sankar:** Conceptualization, Methodology, Supervision, Writing - review & editing. **Ghatu Subhash:** Conceptualization, Methodology, Funding acquisition, Supervision, Writing - review & editing. **Nam Ho Kim:** Methodology, Supervision, Writing - review & editing. **Raphael T. Haftka:** Conceptualization, Methodology, Supervision.

Declaration of Competing Interest

The authors declare that they have no known competing financial interests or personal relationships that could have appeared to influence the work reported in this paper.

Acknowledgements

This research was performed under the Department of Energy (DOE) Nuclear Energy University Programs (NEUP) grant no. DE-NE0008773 to University of Florida. The opinions expressed in this article are solely those of the authors and do not reflect those of the funding agency.

References

[1] Ayranci C, Carey JP. Predicting the longitudinal elastic modulus of braided tubular composites using a curved unit-cell geometry. Compos Part B Eng 2010;41:229–35. https://doi.org/10.1016/j.compositesb.2009.10.006.
[2] Ayranci C, Carey J. 2D braided composites: A review for stiffness critical applications. Compos Struct 2008;85:43–58. https://doi.org/10.1016/j.compstruct.2007.10.004.
[3] De Oliveira Simões JA, Marques AT. Determination of stiffness properties of braided composites for the design of a hip prosthesis. Compos Part A Appl Sci Manuf 2001;32:655–62. https://doi.org/10.1016/S1359-835X(00)00157-3.
[4] Katoh Y, Ozawa K, Shih C, Nozawa T, Shinavski RJ, Hasegawa A, et al. Continuous SiC fiber, CVI SiC matrix composites for nuclear applications: Properties and irradiation effects. J Nucl Mater 2014;448:448–76. https://doi.org/10.1016/j.jnucmat.2013.06.040.
[5] Deck CP, Khalifa HE, Sammuli B, Hilsabeck T, Back CA. Fabrication of SiC-SiC composites for fuel cladding in advanced reactor designs. Prog. Nucl. Energy, vol. 57, Pergamon; 2012, p. 38–45. https://doi.org/10.1016/j.pnucene.2011.10.002.
[6] Karkkainen RL, Sankar BV. A direct micromechanics method for analysis of failure initiation of plain weave textile composites. Compos Sci Technol 2006;66:137–50. https://doi.org/10.1016/j.compscitech.2005.05.018.
[7] Marrey RV, Sankar BV. Micromechanical models for textile structural composites 1995.
[8] Xu L, Kim SJ, Ong CH, Ha SK. Prediction of material properties of biaxial and triaxial braided textile composites. J Compos Mater 2012;46:2255–70. https://doi.org/10.1177/0021998311431353.
[9] Paul RJ, Scott A, Potluri P. Analysis of braided tubes subjected to internal pressure. ICCM Int Conf Compos Mater 2011:1–4.
[10] Aggarwal A, Ramakrishna S, Ganesh VK. Predicting the In-plane Elastic Constants of Diamond Braided Composites. J Compos Mater 2001;35:665–88. https://doi.org/10.1177/002199801772662046.
[11] Carey J, Munro M, Fahim A. Longitudinal Elastic Modulus Prediction of a 2-D Braided Fiber Composite. J Reinf Plast Compos 2003;22:813–31. https://doi.org/10.1177/0731684403022009003.
[12] Chatzigeorgiou G, Efendiev Y, Charalambakis N, Lagoudas DC. Effective thermoelastic properties of composites with periodicity in cylindrical coordinates. Int J Solids Struct 2012;49:2590–603. https://doi.org/10.1016/j.ijsolstr.2012.05.023.
[13] Gélébart L. Conditions aux limites périodiques pour l'homogénéisation numérique de tubes composites. Comptes Rendus - Mec 2011;339:12–9. https://doi.org/10.1016/j.crme.2010.12.010.
[14] Quek SC, Waas AM, Shahwan KW, Agaram V. Analysis of 2D triaxial flat braided textile composites. Int J Mech Sci 2003;45:1077–96. https://doi.org/10.1016/j.ijmecsci.2003.09.003.
[15] Kier ZT, Salvi A, Theis G, Waas AM, Shahwan K. Estimating mechanical properties of 2D triaxially braided textile composites based on microstructure properties. Compos Part B Eng 2015;68:288–99. https://doi.org/10.1016/j.compositesb.2014.08.039.
[16] Marrey RV, Sankar BV. A Micromechanical Model for Textile Composite Plates. J Compos Mater 1997;31.. https://doi.org/10.1177/002199839703101202.
[17] Sankar BV, Marrey RV. A unit-cell model of textile composite beams for predicting stiffness properties. Compos Sci Technol 1993;49:61–9. https://doi.org/10.1016/0266-3538(93)90022-9.
[18] Gibson RF. Principles of Composite Material Mechanics. 2016. https://doi.org/10.1201/b19626.
[19] Hibbit HD, Karlsson BI, Sorensen EP. ABAQUS user manual, version 6.14. Simulia 2014. https://doi.org/10.1577/T09-122.1.
[20] Smith M. ABAQUS/Standard User's Manual, Version 6.9. Dassault Systemes Simulia Corp; 2009.
[21] Whitcomb JD. Three-dimensional stress analysis of plain weave composites. ASTM Spec Tech Publ 1991:417–38. https://doi.org/10.1520/stp17730s.
[22] Eisley JG, Waas AM. Analysis of Structures : An Introduction Including Numerical Methods. Incorporated: John Wiley & Sons; 2011.
[23] Lin H, Brown LP, Long AC. Modelling and simulating textile structures using TexGen. Adv. Mater. Res., vol. 331, Trans Tech Publications Ltd; 2011, p. 44–7. https://doi.org/10.4028/www.scientific.net/AMR.331.44.
[24] Long AC, Brown LP. Modelling the geometry of textile reinforcements for composites: TexGen. Compos. Reinf. Optim. Perform., Elsevier Ltd. 2011:239–64. https://doi.org/10.1533/9780857093714.2.239.
[25] Akpoyomare AI, Okereke MI, Bingley MS. Enforcing periodic boundary conditions on general finite element discretisations of heterogeneous materials. High Perform. Optim. Des. Struct. Mater. II, vol. 1, WIT Press; 2016, p. 129–42. https://doi.org/10.2495/hpsm160121.
[26] Song S, Waas AM, Shahwan KW, Xiao X, Faruque O. Braided textile composites under compressive loads: Modeling the response, strength and degradation. Compos Sci Technol 2007;67:3059–70. https://doi.org/10.1016/j.compscitech.2007.06.008.

[27] Timoshenko S. Strength of Materials, Pt. 2:Advanced Theory and Problems. Krieger Publishing Company; 1983.
[28] Goldsmith MB, Sankar BV, Haftka RT, Goldberg RK. Effects of microstructural variability on thermo-mechanical properties of a woven ceramic matrix composite. J Compos Mater 2015;49:335–50. https://doi.org/10.1177/0021998313519151.
[29] Šmilauer V, Hoover CG, Bažant ZP, Caner FC, Waas AM, Shahwan KW. Multiscale simulation of fracture of braided composites via repetitive unit cells. Eng Fract Mech 2011;78:901–18. https://doi.org/10.1016/j.engfracmech.2010.10.013.